Model Predictive Control for Wake Steering: a Koopman Dynamic Mode Decomposition Approach

Nassir Rodrigues Cassamo
nassir.cassamo@tecnico.ulisboa.pt

Instituto Superior Técnico, Universidade de Lisboa, Lisboa, Portugal

October 2020

Abstract. Sitting wind turbines together in wind farms is economically advantageous. However, as the first turbine extracts energy from the wind, less power is available for downstream turbines. Current industry practices neglect the aerodynamic interaction, optimizing only at the individual turbine level, which leads to suboptimal behaviour of the total wind farm. Controlling wind farms as a whole is becoming increasingly important. Nevertheless, due to the fact that wind farms are high order systems whose dynamics are governed by nonlinear partial differential equations with no known analytical solution, the design and implementation of numerical optimal controllers in high fidelity simulators becomes computationally expensive and unsuitable for real time usage. Reduce order state models provide a possible route to the design and implementation of practical cooperative wind farm controllers. This thesis makes use of an innovative algorithm in the context of wind farm modelling - Input Output Dynamic Mode Decomposition - and the ideas of non linear dynamical system theory - the Koopman Operator - to find suitable reduced order models to be used for model predictive control. The wind farm control strategy of wake redirection control is studied. It is shown that a reduced state space model with 37 states can accurately reproduce the downstream turbine generator power dynamics with a variance accounted for of 88%, rebuild the upstream turbine wake with an average normalized root mean squared error of 4% and that controllers can be designed and implemented in a high fidelity simulator for a collective power reference tracking problem.
Keywords: Wind Farm Control, Wake Redirection Control, Dynamic Mode Decomposition, Koopman Operator Theory, Model Predictive Control.

1. Introduction

The Intergovernmental Panel on Climate Change (IPCC) pointed in 2018 to the climate changes which can be avoided by limiting global warming above pre industrial levels to 1.5^{o}C. The knowledge of the situation's gravity is not new, and since 1995 great emphasis has been placed on the development and use of renewable forms of energy, as stated in the Kyoto Protocol, an international treaty focused on reducing green gas house emissions. Wind energy is one of the fast growing technologies, representing 19% of the total renewable energy production in 2018, compared to 8% in 2010 [22]. Last year alone Europe installed 15.4 GW of new wind power capacity, 28% more than 2018 [14], with offshore wind installations being a record high.

In spite of the economic advantages of sitting wind turbines together in wind farms offshore, the aerodynamic interaction between turbines may have a negative effect on the total electrical power production and may increase loads experienced by turbines. These effects are caused by the wakes, which are flow structures that form behind each turbine. Mitigation of these effects can be achieved by using wind plant control techniques during the operation of the wind farm. The later concept aims at improving the performance of the wind plant as a whole by maximizing the power output of the plant instead of each individual turbine. It was firstly introduced in 1988 in [26], showing that slight increases in the overall energy capture are possible. The assumption that wind farm performance can be increased by operating turbines in the farm at configurations different from their individual optimal control setting has lead to two general control techniques: Wake Redirection Control (WRC) and Axial Induction Control (AIC) [28].

WRC changes the direction of the wake so that its

overlap with downstream rotors can be avoided. It can be achieved by yaw misalignment, which is the focus of this work. By misaligning the rotor, the wind inflow is at an angle to the rotor axis, and the thrust force is divided into its components: f_x is parallel to the rotor and slows the wind and f_y is perpendicular and applies the force which causes the wake to be redirected. This strategy has been proved to yield good results in simulations, wind tunnel experiments and field tests. High fidelity simulations have showed significant redirection effects coupled with reductions in loading [7]. Wind tunnel tests have reproduced promising results, with [5] showing up power increases of up to 12%. Recent field tests in a commercial wind farm in Italy [8] measured increases up to 35% for two turbine interactions and up to 16% for three turbine interactions, although power losses were also registered for certain wind directions.

Finding the optimal control settings in wind turbines that account for the aerodynamic interaction at the wind farm level in real time has thus become a challenging and active topic of research. The work in [18, 19] provides an optimal control framework for dynamic induction control. The model predictive control approach employed, in which the wind farm boundary layer is modelled using large-eddy simulations (LES) of the Navier Stokes partial differential equations (PDEs) provide benchmark results that yield insight into the potential of wind farm control. Nevertheless, the high computational cost makes it unsuitable as a real controller. Reduced order state models (ROMs) provide a possible route to the real-time implementation of optimal dynamic controllers by leveraging model order reduction techniques.

Proper Orthogonal Decomposition (POD) and Dynamic Mode Decomposition (DMD) are two examples of such techniques. In [11] a DMD model is embedded in a Kalman filter and it is shown that the entire wake flow can be predicted with a global accuracy of 4%. This application, however, is only for a single turbine. A two turbine setting appears in [29], where the findings indicate that a ROM can be obtained and used as a predictive model where a forced input is used. Furthermore, in [1], a Linear Quadratic Gaussian (LQG) controller designed with a ROM is used to control the thrust of the downstream turbine and it is shown that the later is able to achieve the control objective of decreasing the spanwise velocity fluctuations at a point downstream of the turbines.

The contributions of this work are three fold: (1) it is shown that ROMs can be derived based on DMD techniques and possibly improved by capitalising on ideas of non linear dynamical systems theory (2) that the models are able to reproduce the generator power in two turbines separated by 5 rotor diameters with a Variance Accounted For (VAF) of 88% and reproduce the wake with an average Normalized Root Mean Squared Error (NRMSE) of 4%, both for validation data and (3) that it can be used to track a specific collective power reference signal in a high fidelity Computational Fluid Dynamics (CFD) simulator.

This paper is divided into five sections: section 2 introduces the mathematical reduced order modelling techniques. These are then used in section 3 where the ROM for yaw control is derived and the power reference tracking problem presented. Section 4 summarizes the main results obtained by testing it in a high fidelity simulator. Conclusions and future research directions are then discussed in section 5.

2. Reduced Order Modelling

2.1. Input Output Dynamic Mode Decomposition

DMD method firstly originated in the fluid dynamic community as a means to decompose complex flows into a simple representation, published in [24]. Since then, different variations of DMD have surged [10]. DMD role is to extract meaningful spatio temporal patterns that dominate dynamic activity in high dimensional non linear systems. DMD has been applied to a wide variety of flow geometries and it has proven its value as a new quantitative flow analysis tool when compared to other methods. It is shown in [25] whereas POD concentrates on the more energetic structures of the flow, DMD isolates the less energetic but more unstable axial vorticity patterns, which may be dynamically more relevant.

The standard DMD algorithm has been successfully applied to high dimensional non linear systems in the context of data interpolation in several different domains, such as epidemiology [20] and neuroscience [4], shedding light on their dynamical properties. In the context of control, DMD has been developed to account for exogenous inputs [21] and input-output information. This approach, detailed in [2, 3], referred to as Input Output Dynamic Mode Decomposition (IODMD), combines DMD with standard subspace identification often used in the controls literature [12] to obtain a characterization of the system.

In the DMD framework, data is collected from a dynamical system

$$\frac{d\boldsymbol{x}}{dt} = \mathbf{f}(\boldsymbol{x}; t; \mu) \tag{1}$$

where $\boldsymbol{x}(t) \in \mathbb{R}^n$ is a vector representing the state

of the dynamical system at time t, μ contains parameters of the system and **f (·)** represents the dynamics. Resorting to the equation free perspective, data measurements of the system alone are used to approximate the dynamics. The approximated linear dynamical system can be constructed in discrete-time, sampling the analogous continuous time system every Δt. Inputs and outputs are accounted by using the state space representation of a linear time invariant (LTI) dynamical system:

$$\begin{aligned} \boldsymbol{x}_{k+1} &= \mathbf{A}\boldsymbol{x}_k + \mathbf{B}\boldsymbol{u}_k \\ \boldsymbol{y}_k &= \mathbf{C}\boldsymbol{x}_k + \mathbf{D}\boldsymbol{u}_k \end{aligned} \tag{2}$$

where $\boldsymbol{x}_k \in \mathbb{R}^n$, $\boldsymbol{u}_k \in \mathbb{R}^q$ and $\boldsymbol{y}_k \in \mathbb{R}^l$ are the state, input and output vectors respectively. Matrices $\mathbf{A} \in \mathbb{R}^{n\times n}$, $\mathbf{B} \in \mathbb{R}^{n\times q}$, $\mathbf{C} \in \mathbb{R}^{l\times n}$ and $\mathbf{D} \in \mathbb{R}^{l\times q}$ are the state matrices that together form the state space representation. The IODMD algorithm can be divided into three distinct steps:

1. Organize snapshot matrices: the series of data containing relevant information of the three dimensional vector flow field at each time instant k is taken and flatten into a single column vector $\boldsymbol{x}_k$, referred to as a snapshot of data. All time instants are then combined into one single matrix which is then divided into the data matrix **X** and its time shifted version **X'**:

$$\mathbf{X} = \begin{bmatrix} | & | & & | \\ \boldsymbol{x}_1 & \boldsymbol{x}_2 & \cdots & \boldsymbol{x}_{m-1} \\ | & | & & | \end{bmatrix} \quad \mathbf{X'} = \begin{bmatrix} | & | & & | \\ \boldsymbol{x}_2 & \boldsymbol{x}_3 & \cdots & \boldsymbol{x}_{m} \\ | & | & & | \end{bmatrix} \tag{3}$$

where the number of rows n is equal to the number of spatial points saved per time snapshot and the number of columns m is equal to the number of snapshots taken. The input $\boldsymbol{\Upsilon}$ and output **Y** snapshot matrices are similarly gathered:

$$\boldsymbol{\Upsilon} = \begin{bmatrix} | & | & & | \\ \boldsymbol{u}_1 & \boldsymbol{u}_2 & \cdots & \boldsymbol{u}_{m-1} \\ | & | & & | \end{bmatrix} \quad \mathbf{Y} = \begin{bmatrix} | & | & & | \\ \boldsymbol{y}_1 & \boldsymbol{y}_2 & \cdots & \boldsymbol{y}_{m-1} \\ | & | & & | \end{bmatrix} \tag{4}$$

2. Take Singular Value Decomposition of X: by appropriately choosing a truncation value r of the number of singular values to retain in the Singular Value Decomposition (SVD), **X** can be factorized as $\mathbf{U\Sigma V}^*$, where $\mathbf{U} \in \mathbb{C}^{n\times r}$, $\boldsymbol{\Sigma} \in \mathbb{C}^{r\times r}$, $\mathbf{V}^* \in \mathbb{C}^{r\times m-1}$ and * is the conjugate transpose.

3. Formulate least squares problem by projecting system to reduced dimension space: Equation (2) is then rewritten in terms of the snapshot matrices in (3) and (4) in the following compact format:

$$\begin{bmatrix} \mathbf{X'} \\ \mathbf{Y} \end{bmatrix} = \begin{bmatrix} \mathbf{A} & \mathbf{B} \\ \mathbf{C} & \mathbf{D} \end{bmatrix} \begin{bmatrix} \mathbf{X} \\ \boldsymbol{\Upsilon} \end{bmatrix} \tag{5}$$

The state is then projected onto the subspace defined by an orthonormal basis. A suboptimal but useful choice for the projection space is given by the POD modes of **X**, as in standard DMD. By taking the SVD of **X** given by $\mathbf{X} \approx \mathbf{U\Sigma V}^*$ with a truncation value r, the columns of **U** specify the orthonormal basis to project the high order state. The low order state matrices are then $\tilde{\mathbf{A}} = \mathbf{U}^*\mathbf{AU}$, $\tilde{\mathbf{B}} = \mathbf{U}^*\mathbf{B}$, $\tilde{\mathbf{C}} = \mathbf{CU}$ and $\tilde{\mathbf{D}} = \mathbf{D}$. These equivalences can be rewritten in terms of the high order matrices **A**, **B**, **C** and **D**: $\mathbf{A} = \mathbf{U}\tilde{\mathbf{A}}\mathbf{U}^*$, $\mathbf{B} = \mathbf{U}\tilde{\mathbf{B}}$, $\mathbf{C} = \tilde{\mathbf{C}}\mathbf{U}^*$ and $\mathbf{D} = \tilde{\mathbf{D}}$. Substituting in (5) and rearranging, the reduced order state matrices are obtained by minimizing the error of the Frobenius norm [9]:

$$\min_{\left[\begin{smallmatrix} \tilde{\mathbf{A}} & \tilde{\mathbf{B}} \\ \tilde{\mathbf{C}} & \tilde{\mathbf{D}} \end{smallmatrix}\right]} \left\| \begin{bmatrix} \mathbf{X'} \\ \mathbf{Y} \end{bmatrix} - \begin{bmatrix} \mathbf{U} & \mathbf{0} \\ \mathbf{0} & \mathbf{I} \end{bmatrix} \begin{bmatrix} \tilde{\mathbf{A}} & \tilde{\mathbf{B}} \\ \tilde{\mathbf{C}} & \tilde{\mathbf{D}} \end{bmatrix} \begin{bmatrix} \mathbf{U}^* & \mathbf{0} \\ \mathbf{0} & \mathbf{I} \end{bmatrix} \begin{bmatrix} \mathbf{X} \\ \boldsymbol{\Upsilon} \end{bmatrix} \right\|_F^2 \tag{6}$$

where $\tilde{\mathbf{A}} \in \mathbb{R}^{r\times r}$, $\tilde{\mathbf{B}} \in \mathbb{R}^{r\times q}$, $\tilde{\mathbf{C}} \in \mathbb{R}^{l\times r}$, and $\tilde{\mathbf{D}} \in \mathbb{R}^{l\times q}$. The reduced order state matrices are then obtained by least squares, taking into account that the reduced order representation of **X** and **X'** are respectively $\mathbf{U}^*\mathbf{X'}$ and $\boldsymbol{\Sigma}\mathbf{V}$:

$$\Theta_{\text{IODMD}} = \begin{bmatrix} \tilde{\mathbf{A}} & \tilde{\mathbf{B}} \\ \tilde{\mathbf{C}} & \tilde{\mathbf{D}} \end{bmatrix} = \begin{bmatrix} \mathbf{U}^*\mathbf{X'} \\ \mathbf{Y} \end{bmatrix} \begin{bmatrix} \boldsymbol{\Sigma}\mathbf{V} \\ \boldsymbol{\Upsilon} \end{bmatrix}^{\dagger} \tag{7}$$

Using this methodology, an accurate mapping for input-output information can be obtained, as well as an approximation of the full order state, by $\boldsymbol{x}_k = \mathbf{U}\tilde{\boldsymbol{x}}_k$.

2.2. Koopman Operator theory

The Koopman operator, firstly introduced in [15] and then recently resurged in the context of modern data-driven dynamical systems, is defined as an infinite-dimensional linear operator that evolves fields of physical observables defined on a state space of a dynamical system. More explicitly, let the generic dynamical system in equation (1) be again considered, and defined on a state space **M**. This induces a discrete-time dynamical system given by the flow map $\mathbf{F}_t : \mathbf{M} \to \mathbf{M}$, $\boldsymbol{x}_{k+1} = \mathbf{F}_t(\boldsymbol{x}_k)$. A function defined as $g : M \to \mathbb{R}$ is called an observable of the system. The Koopman operator $\mathcal{K}_t$ acts on observable functions g as $\mathcal{K}_t = g \circ \mathbf{F}_t$ where $\circ$ is the composition operator, so that:

$$\mathcal{K}_t g(\boldsymbol{x}_k) = g(\mathbf{F}_t(\boldsymbol{x}_k)) = g(\boldsymbol{x}_{k+1}) \tag{8}$$

$$g(\boldsymbol{x}_{k+1}) = \mathcal{K}_t g(\boldsymbol{x}_k) \tag{9}$$

It is now evident in (9) that the observation of the state, or, in other words, a function of the measured state variable, is advanced to the next time step by the Koopman operator. This is true for *any* observable function and for *any* point $\boldsymbol{x}_k \in \mathbf{M}$, hence the infinite-dimension.

The spectral decomposition of the Koopman operator is instrumental in representing solutions to

a dynamical system of interest. Considering the eigenvalue problem $\mathcal{K}\varphi_k = \lambda_k\varphi_k$, the functions $\varphi_k(\boldsymbol{x})$ are called Koopman eigenfunctions and they define a set of intrinsic measurement coordinates, on which it is possible to advance these measurements with a linear dynamical system. The new measurement space formed by a vector of observables $\boldsymbol{g}(\boldsymbol{x})$ can be expressed in terms of the Koopman eigenfunctions:

$$\boldsymbol{g}(\boldsymbol{x}) = \begin{bmatrix} g_1(\boldsymbol{x}) \\ \vdots \\ g_p(\boldsymbol{x}) \end{bmatrix} = \sum_{k=1}^{\infty} \varphi_k(\boldsymbol{x})\boldsymbol{v}_k \tag{10}$$

where $\boldsymbol{v}_k$ is the kth Koopman mode of the map **F** corresponding to the observable $\boldsymbol{g}$, associated with the kth Koopman eigenfunction, i. e., the weighting of each observable on the eigenfunction. The expression in (10) can be interpreted as a linear combination of the eigenfunctions φ_k of $\mathcal{K}$ where $\boldsymbol{v}_k$ is the coefficient in the expansion. The nonlinear system can either be evolved in the original state space or in the measurement space as in (10).

$$\begin{aligned} \mathcal{K}\sum_{k=1}^{\infty} \varphi_k(\boldsymbol{x})\boldsymbol{v}_k &= \sum_{k=1}^{\infty} \mathcal{K}\varphi_k(\boldsymbol{x})\boldsymbol{v}_k \\ &= \sum_{k=1}^{\infty} \lambda_k\varphi_k(\boldsymbol{x})\boldsymbol{v}_k \end{aligned} \tag{11}$$

Future solutions can be computed by multiplication with the Koopman eigenvalues, $\lambda_k \in \mathbb{C}$, which characterize the temporal behaviour of the corresponding Koopman mode $\boldsymbol{v}_k$.

The connections of DMD to the underlying non linear dynamics of a system through the Koopman operator theory were firstly established in [23], where it is shown that DMD produces approximations to eigenvalues of the Koopman operator, and their corresponding modes. DMD is thus a manifestation of Koopman theory for the specific case when the observable functions are the identity or a linear transformation of the underlying state space. Approaches combining DMD with the ideas of the Koopman operator by augmenting DMD to include a richer set of non-linear observables and find the best set of coordinates to describe the non linear dynamics have since been developed [13, 30]. An alternative approach is to select a parsimonious set of observables based upon knowledge of the physics of the system, as described in [16] and proved to yield better results when compared to POD for prediction purposes [17].

The ideas of the Koopman operator are explored in the context of wind farm control, in the sense that the best coordinates to describe the evolution of the system's dynamics are investigated.

3. Modelling

3.1. Reduced Order Model for yaw control

The system of interest is a small wind farm, where two turbines are placed apart. The direct manipulated variable is the yaw angle of the upstream turbine and the outputs are the generator powers of both turbines, as schematically represented in Fig.1.

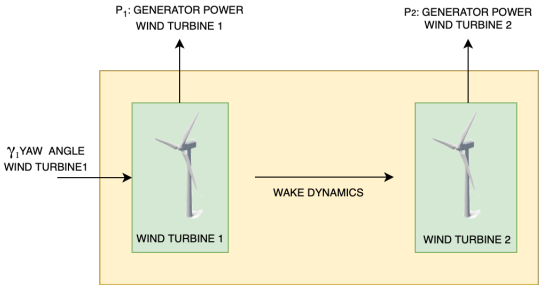

Figure 1: Wind farm system with one input - first turbine yaw angle - and two outputs - power generated in both turbines.

The input output data set to be used for IODMD is obtained by performing a CFD simulation in Software for Offshore Wind Farm Applications (SOWFA). SOWFA is a LES of the three-dimensional wind flow around one or more turbine rotors in the ABL developed by the United States National Renewable Energy Laboratory (NREL). In the LES method, in order to limit the computational cost of the simulation, the larger scales of the flow field are resolved by solving the temporally and spatially unsteady Navier-Stokes equations. The rotating rotor blades are modelled through an actuator line approach. The actuator lines are coupled with the FAST turbine aeroelastic simulator tool which calculates the loads, power and rotor speed of each turbine. SOWFA is a widely used tool in the literature to obtain accurate data and more information is available in [6].

In this work, wind with a uniform inflow profile is used to demonstrate the working principles of IODMD. The case of a wind farm with two turbines is studied to assess the gain in energy in the second one. The downstream turbine is situated 5 rotor diameters (5D) behind the upstream turbine. The turbine used for the simulation is the DTU 10MW turbine, with a rotor diameter of 178.3 [m]. Detailed design characteristics can be found in [31]. The domain size has dimensions of approximate 1.71 [km] in the x direction, 343 [m] in the y direction and 300 [m] in the z direction. A total of 550 points in x, 111 points in y and 99 points in z are sampled during the simulation. A total of 6 million points, each one containing information on the (u, v, w) velocity components is taken. A pre processing step of the data is performed in a cluster,

aiming to retrieve only information at each fourth point, decreasing the total number of points from 6 million to roughly 100 thousand samples, decreasing computational effort. Flow field information is sampled at each 2 seconds. In addition to flow field data, information of the blades, nacelle, rotor, tower and generator power is saved. These information is sampled at each 0.2 seconds.

Randomized Binary Signals (RBS) of the yaw angle of the first turbine γ_{t1} serve as inputs. The yaw angle is first set to -10 degrees, and then varied to -30 degrees randomly throughout the simulation. The yaw of the second turbine γ_{t2} remains the same throughout the simulation. The powers generated at the upstream and downstream turbines vary as the control settings change and the wake deflects. These variations can be seen in Fig.2 and Fig.3.

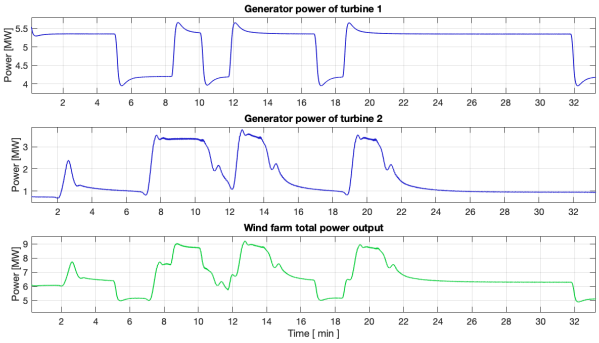

Figure 2: Generator power variations of both turbines (in blue) during simulation and total generated power (in green).

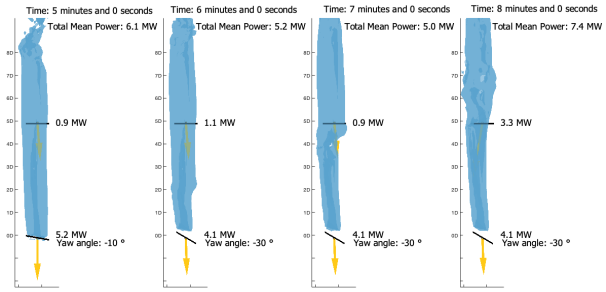

Figure 3: Wake deflection dynamics as upstream turbine increases yaw angle. The absolute vorticity isosurface of value 5.65 is represented.

In Fig.2 the effectiveness of the wind farm control strategy can be observed. The yaw angle setting to -10 degrees leads to the upstream turbine capturing 5.35 [MW] and the downstream turbine 0.96 [MW], a total of 6.26 [MW]. By further yawing the turbine to -30 degrees a total of approximate 7.56 [MW] is captured. This increased is explained by the deflection of the wake as Fig.3 illustrates. The first turbine is sacrificed, generating only 4.20 [MW]. Nevertheless the second one compensates by capturing 3.36 [MW].

Three pre processing steps are performed before using simulation data for the systems identification task: (1) only flow field information between first and second turbine is used (2) turbine information is resampled to be consistent with flow field data (3) trends and offsets are manually removed from data. The input output information, used for identification and validation of the models, is depicted in Fig.4.

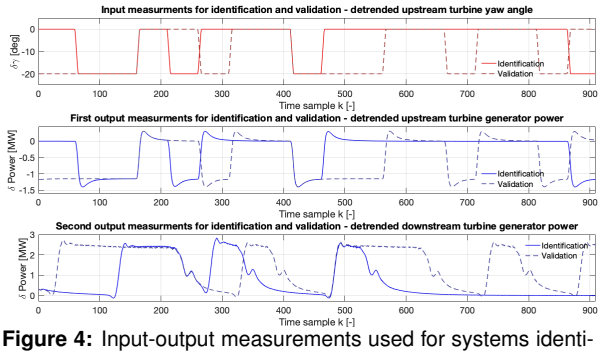

Figure 4: Input-output measurements used for systems identification (solid line) and model validation (dashed line).

The streamwise velocity component u is firstly used to derive the IODMD model, referred to as IODMD$_u$. A truncation value r of 100 is used, and singular values are increasingly added to build models. The VAF of both outputs for each model computed is represented in Fig.5. Power generator in the second turbine presents more complex dynamic and requires more states (also referred to as modes within the context of DMD).

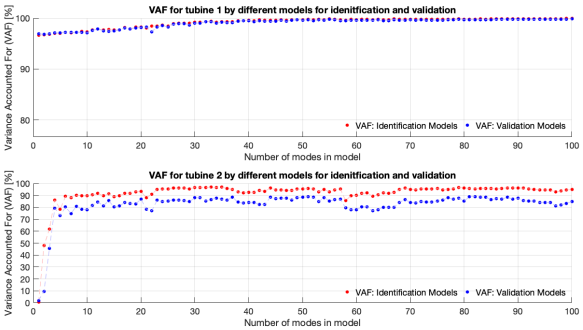

Figure 5: VAF of each model computed. Each model has increasing number of sates from left to right.

The best performing model is able to reproduce the generator power dynamics at the upstream turbine with a VAF of 99.12% and at the downstream turbine with a VAF of 88.40%, as represented in Fig.6. The IODMD$_u$ chosen has 37 states.

Fig.7 puts in evidence the ability of a linear state space reduced order model with 37 states to reproduce the non linear dynamics of a wind turbine wake with tens of thousands of states. Minor differences are visible in the each snapshots. Taken

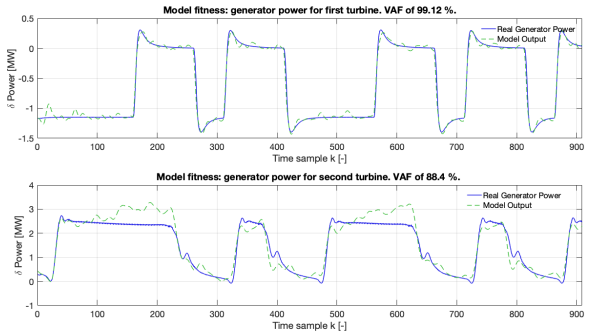

Figure 6: SOWFA detrended turbine generator power information (blue) and best IODMD$_u$ model performance (green).

together, for every time instant of the simulation, such differences represent an average NRMSE of 4%, using validation data.

The model's reconstruction capabilities are further illustrated in Fig.8. In the later, the wake is rebuilt at the downstream turbine rotor plane for key instances when the modified wake travels downstream.

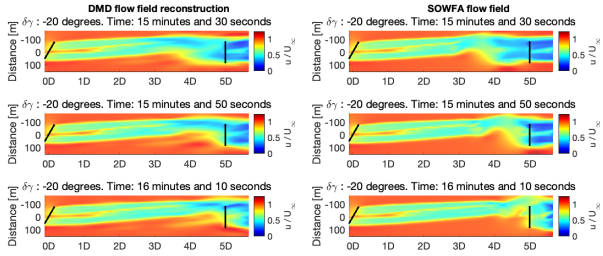

Figure 7: High order state reconstruction based on evolution of low order states (left) and SOWFA validation data (right). Reconstruction at hub height plane.

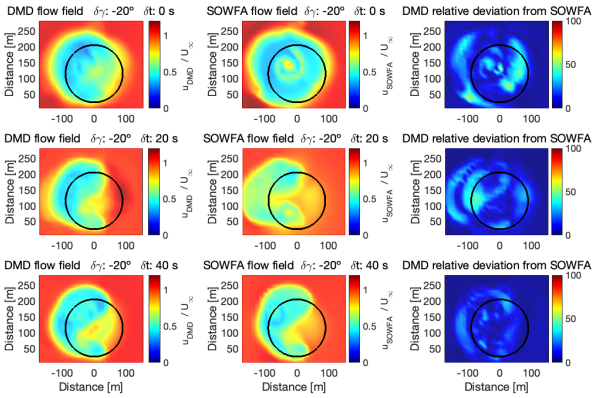

Figure 8: Comparison of flow field reconstruction at downstream turbine rotor plane at different instances. IODMD$_u$ flow field deviation with relation to SOWFA data is shown on the right.

In light of the Koopman operator theory, several variables are used for the high order states, testing the hypothesis that other coordinates might be better suited to describe the dynamics. The results of the several variables used to build and validate models are summarized in Table 1. The best model for each observable used is chosen based on the highest VAF for the downstream turbine generator power, and compared to the IODMD$_u$. VAF(WT1)$|_r$ corresponds to VAF of the upstream turbine generator power for the chosen model.

Model properties	Model obtained by IODMD			Δ IODMD$_u$	
Observable	VAF(WT2)$_{\max}$	Model size	VAF(WT1)$|_r$	Δ VAF (WT2)$_{max}$	Δ size
v	87.12 %	40	99.39 %	-1.28%	+8.11%
w	87.54 %	50	99.35 %	-0.86%	+35.14%
u'	78.14 %	38	98.08 %	-10.26%	+2.70%
v'	61.30 %	31	97.13 %	-27.10%	-16.22%
u^2	89.63 %	26	98.83 %	**+1.23%**	**-29.73%**
v^2	89.58 %	12	97.52 %	**+1.18%**	**-67.57%**
w^2	87.85 %	47	97.67 %	-0.55%	+27.03%
$u \cdot v$	69.40 %	15	97.58 %	-19.00%	-59.46%
$u^2 + v^2$	89.42 %	26	98.84 %	+1.02%	-29.73%
$u^2 + v^2 + w^2$	89.36 %	49	99.75%	+0.96%	+32.43%

Table 1: Models validation results using different observables.

Using the non linear observable u^2 appears to both increase the VAF in 1.23% and decrease the number of states needed to accurately incorporate the generator power dynamics from 37 to 26. Other observables provide similar benefits, indicating that better coordinates to describe the dynamics in hand may exist.

Despite different observables used, the best performing models share some similarities in their frequency response, presenting resonance peaks around the same (adimensionalized) frequencies of 0.21, 0.59 and 0.69 Strouhal.

3.2. Model Predictive Control

The control problem to be formulated is a reference tracking problem, where the wind farm system has to produce a specified collective power in order to assess gains at the plant level. To accomplish that, a predictive controller is designed so that the two turbines can work together by taking the aerodynamic effect into consideration.

The IODMD$_{u^2}$ model is used to design a Model Predictive Controller (MPC). The Incremental Input Output (IIO) model is used, where the increments of the input signal are applied to the models instead of the input directly, as described in [27]. The standard state space model is rewritten in terms of incremental variables, and the extended state space is formulated, so that the state is now $\boldsymbol{x}_k^e = \begin{bmatrix} \boldsymbol{y}_{k-1} & \Delta \boldsymbol{x}_k \end{bmatrix}^T$ and the state space matrices $\mathbf{A}_e, \mathbf{B}_e, \mathbf{C}_e$, are defined as follows in (12):

$$\begin{bmatrix} \boldsymbol{y}_k \\ \Delta \boldsymbol{x}_{k+1} \end{bmatrix} = \begin{bmatrix} \mathbf{I} & \mathbf{C} \\ \mathbf{0} & \mathbf{A} \end{bmatrix} \begin{bmatrix} \boldsymbol{y}_{k-1} \\ \Delta \boldsymbol{x}_k \end{bmatrix} + \begin{bmatrix} \mathbf{0} \\ \mathbf{B} \end{bmatrix} \Delta \boldsymbol{u}_k$$
$$\boldsymbol{y}_k = \begin{bmatrix} \mathbf{I} & \mathbf{C} \end{bmatrix} \begin{bmatrix} \boldsymbol{y}_{k-1} \\ \Delta \boldsymbol{x}_k \end{bmatrix} \tag{12}$$

Future predictions computed by the model can be written in the compact format $\bar{\mathbf{P}} = \bar{\mathbf{H}}_e \Delta\bar{\mathbf{U}} + \mathbf{\Gamma}_e \boldsymbol{x}_k^e$, where $\bar{\mathbf{P}}$ are the generator power of both turbines (outputs $\boldsymbol{y}_k$) computed for the prediction horizon H_p, $\begin{bmatrix}\mathbf{P}_{k+1} & \mathbf{P}_{k+2} & \cdots & \mathbf{P}_{k+H_p}\end{bmatrix}^T$, $\Delta\bar{\mathbf{U}}$ are the incremental control actions over the control horizon H_c, $\begin{bmatrix}\Delta u_k & \Delta u_{k+1} & \cdots & \Delta u_{k+H_p-1}\end{bmatrix}^T$. Matrices $\bar{\mathbf{H}}_e$ and $\mathbf{\Gamma}_e$ are defined as follows:

$$\bar{\mathbf{H}} = \begin{bmatrix} \mathbf{C}_e\mathbf{B}_e & \mathbf{0} & \cdots & \mathbf{0} \\ \mathbf{C}_e\mathbf{A}_e\mathbf{B}_e & \mathbf{C}_e\mathbf{B}_e & \cdots & \mathbf{0} \\ \vdots & \vdots & \ddots & \vdots \\ \mathbf{C}_e\mathbf{A}_e^{H_p-1}\mathbf{B}_e & \mathbf{C}_e\mathbf{A}_e^{H_p-2}\mathbf{B}_e & \cdots & \mathbf{C}_e\mathbf{B}_e \end{bmatrix} \tag{13}$$

$$\mathbf{\Gamma} = \begin{bmatrix} \mathbf{C}_e\mathbf{A}_e \\ \mathbf{C}_e\mathbf{A}_e^2 \\ \vdots \\ \mathbf{C}_e\mathbf{A}_e^{H_p} \end{bmatrix} \tag{14}$$

A cost function J penalizing the reference tracking and control action is defined, where $\mathbf{Q}$ and $\mathbf{R}$ are relative weights of reference deviation and input usage, respectively. The collective power of both turbines $\hat{\mathbf{P}}$ predicted by the model is compared to a pre defined reference $\mathbf{P}_{ref}$ to be tracked.

$$J = (\hat{\mathbf{P}} - \mathbf{P}_{ref})^T\mathbf{Q}(\hat{\mathbf{P}} - \mathbf{P}_{ref}) + \Delta\bar{\mathbf{U}}^T\mathbf{R}\Delta\bar{\mathbf{U}} \tag{15}$$

The power outputs of each turbine are combined to assess total power production by making use of matrix $\mathbf{F} \in \mathbb{R}^{H_p \times l \cdot H_p}$:

$$\mathbf{F} = \begin{bmatrix} 1 & 1 & 0 & 0 & \cdots & 0 & 0 \\ 0 & 0 & 1 & 1 & \cdots & 0 & 0 \\ \vdots & \vdots & \vdots & \vdots & \ddots & \vdots & \vdots \\ 0 & 0 & 0 & 0 & \cdots & 1 & 1 \end{bmatrix} \tag{16}$$

Inserting the future predictions of the IIO MPC by making use of matrices in (13), (14) and $\mathbf{F}$, the cost function becomes:

$$\begin{aligned} J = (&\mathbf{F}\bar{\mathbf{H}}_e\Delta\bar{\mathbf{U}} + \mathbf{F}\mathbf{\Gamma}_e\boldsymbol{x}_k^e - \mathbf{P}_{ref})^T\mathbf{Q}(\mathbf{F}\bar{\mathbf{H}}_e\Delta\bar{\mathbf{U}} \\ &+ \mathbf{F}\mathbf{\Gamma}_e\boldsymbol{x}_k^e - \mathbf{P}_{ref}) + \Delta\bar{\mathbf{U}}^T\mathbf{R}\Delta\bar{\mathbf{U}} \end{aligned} \tag{17}$$

The cost function can be further simplified, by observing that a constant term appears $\mathcal{C} = \mathbf{F}\mathbf{\Gamma}_e\boldsymbol{x}_k^e - \mathbf{P}_{ref}$:

$$\begin{aligned} J = &(\mathbf{F}\bar{\mathbf{H}}_e\Delta\bar{\mathbf{U}} + \mathcal{C})^T\mathbf{Q}(\mathbf{F}\bar{\mathbf{H}}_e\Delta\bar{\mathbf{U}} + \mathcal{C}) \\ &+ \Delta\bar{\mathbf{U}}^T\mathbf{R}\Delta\bar{\mathbf{U}} \end{aligned} \tag{18}$$

Making use of the mathematical properties of matrices, the expression in (18) can be further simplified and rewritten as follows:

$$\begin{aligned} J = &\Delta\bar{\mathbf{U}}^T(\bar{\mathbf{H}}_e^T\mathbf{F}^T\mathbf{Q}\mathbf{F}\bar{\mathbf{H}}_e + \mathbf{R})\Delta\bar{\mathbf{U}} + \\ &2\Delta\bar{\mathbf{U}}^T\bar{\mathbf{H}}_e^T\mathbf{F}^T\mathbf{Q}\mathcal{C} + \mathcal{C}^T\mathbf{Q}\mathcal{C} \end{aligned} \tag{19}$$

The minimisation of the cost function in (19) can be rewritten as a quadratic optimization problem of the type:

$$\begin{aligned} \Delta\bar{\mathbf{U}}* = \min_{\Delta\bar{\mathbf{U}}} &\left\{\frac{1}{2}\Delta\bar{\mathbf{U}}^T\mathcal{H}\Delta\mathbf{U} + \boldsymbol{f}^T\Delta\mathbf{U}\right\}, \\ &\text{subject to : } \mathbf{M}\Delta\bar{\mathbf{U}} \leq \mathbf{\Lambda} \end{aligned} \tag{20}$$

where $\mathcal{H}$ and $\boldsymbol{f}$ are taken from the cost function formulation (19), $\mathcal{H} = 2(\bar{\mathbf{H}}_e^T\mathbf{F}^T\mathbf{Q}\mathbf{F}\bar{\mathbf{H}}_e + \mathbf{R})$ and $\boldsymbol{f} = 2(\bar{\mathbf{H}}_e^T\mathbf{F}^T\mathbf{Q}(\mathbf{F}\mathbf{\Gamma}_e\boldsymbol{x}_k^e - \mathbf{P}_{ref}))$.

Matrices $\mathbf{M}$ and $\mathbf{\Lambda}$ are used to define inequality constraints for the optimisation problem. They are defined such that the yaw angle is restricted to a vicinity of the linearisation point used:

$$-35 \leq \gamma_{t1} \leq 0 \tag{21}$$

Predictive control uses the receding horizon principle, meaning that after computing the optimal control sequence over the defined control horizon Hc, only the first control sample is implemented. This results in a new control setting for the first turbine. The horizon is then shifted one time sample and the optimization is restarted with new information on the measurements.

4. Implementation in SOWFA

The controller is then tested in SOWFA. The parameters are firstly tuned. The prediction horizon H_p and control horizon H_c are kept the same for simplicity purposes. A prediction horizon of at least 300 time samples should be used so that the slow dynamics of the travelling wake can be taken into account and the two turbines can work in a cooperative fashion to follow the collective power reference, as depicted in Fig.9.

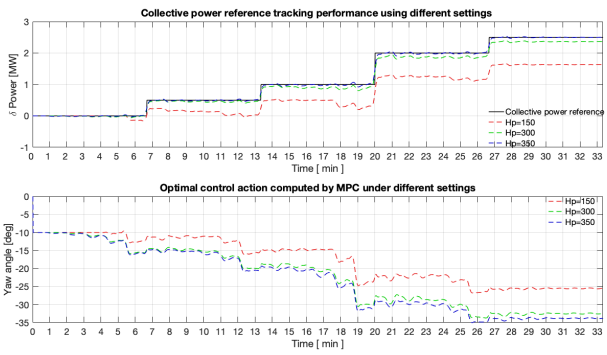

Figure 9: Predictive controller performance for collective power reference tracking using different values for the prediction and control horizons.

The tracking penalty matrix $\mathbf{Q}$ entries are equal to 10 and the control action penalty matrix $\mathbf{R}$ are equal to 1. These values were found to provide a

satisfactory balance between tracking performance and control action in further simulations. Based on the parameters found, $Hp = Hc = 300$, $\mathbf{Q} = 10$ and $\mathbf{R} = 1$, an open loop implementation of the controller in SOWFA in performed. The results are summarized in Fig.10.

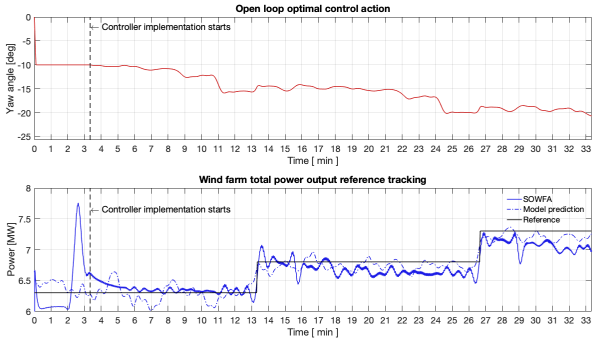

Figure 10: Open-loop predictive controller performance for collective power reference tracking implemented in SOWFA.

It is shown in Fig.10 that the predictive controller enables a cooperative action, in the sense that before a new collective power reference sets in (around minute 13, for example), the yaw angle is manipulated beforehand, almost two minutes before (around minute 11, as depicted in the upper graph of Fig.10).

The discrepancies between the model's predictions and results from SOWFA can in part be explained by the existing non linearities. The power of the first turbine is underestimated and the power of the second turbine overestimated, leading to an overestimation by the model of the total power produced, as illustrated in the last graph of Fig.11.

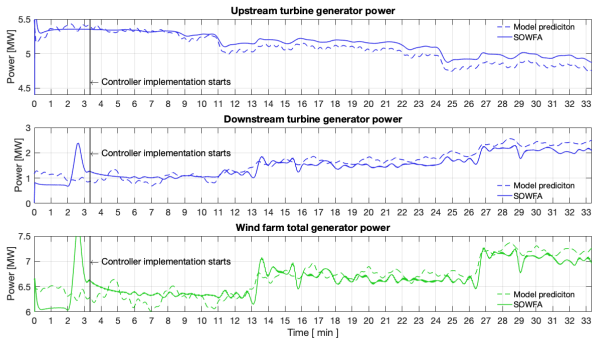

Figure 11: Open-loop implementation of MPC in SOWFA for tracking a collective power reference. Analysis of each turbine power production.

The mismatch between model predictions and true measurements is corrected in the final implementation of the controller. The closed loop implementation is achieved by designing an observer that estimates the states based on SOWFA measurements which the MPC makes use of to compute the control action, as schematically represented in Fig.12.

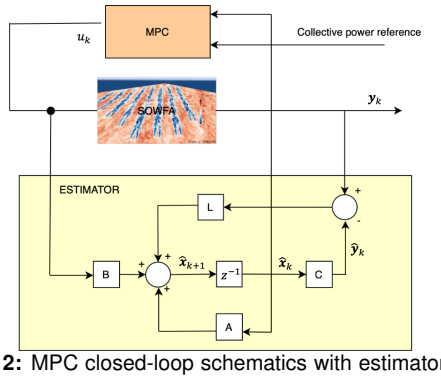

Figure 12: MPC closed-loop schematics with estimator implementation for final simulation in SOWFA.

The results of the closed loop simulation in SOWFA are depicted in Fig.13. The final controller settings are used: Hp = Hc = 350, **Q**=10 and **R**=1. The yaw angle is restricted to 0 and -35 degrees and the yaw angle rate is constrained to values between -0.25 and 0.25. The later restriction is set to avoid aggressive control actions as a consequence of state estimation. The controller is implemented after the first 50 seconds of simulation. The oscillations in collective power are due to fluctuations in generator power at the downstream turbine, as Fig.14 portrays.

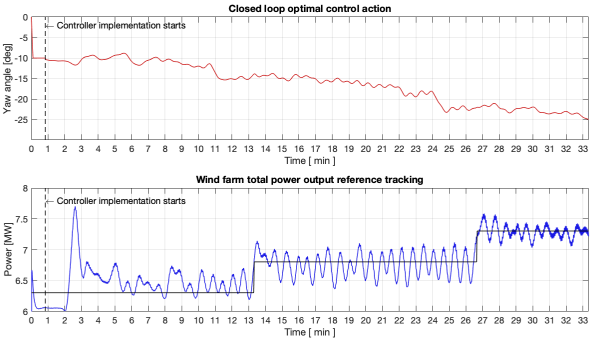

Figure 13: Closed-loop predictive controller performance for collective power reference tracking implemented in SOWFA.

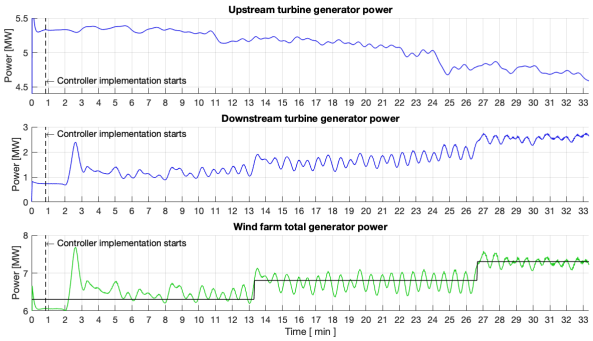

Figure 14: Closed-loop predictive controller performance for collective power reference tracking implemented in SOWFA.

In order to reduce oscillations in power produced and improve the smoothness of the tracking solution, further restrictions are imposed on the yaw angle rate. Two additional and final simulations are carried out, where the rate is restricted to values between -0.1 and 0.1 and between -0.05 and 0.05. The upstream turbine yaw angle and its corresponding rate of change are illustrated in Fig.15.

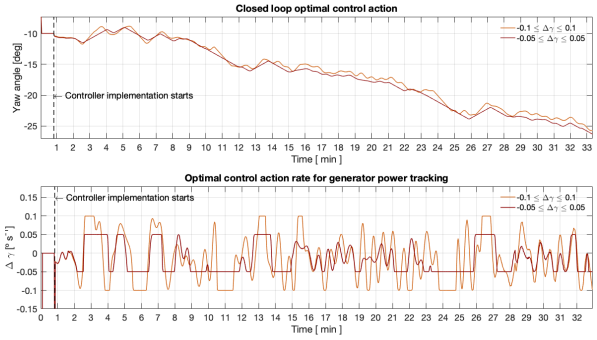

Figure 15: Closed-loop predictive controller performance regarding control action effort.

As a consequence of a smoother control action, less oscillations in terms of produced power at the downstream turbine are measured, as Fig.16 illustrates. Therefore, the collective power reference can be tracked satisfactory while simultaneously avoiding large fluctuations in total produced power.

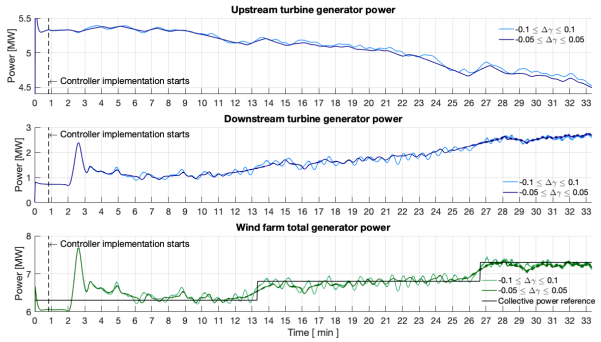

Figure 16: Closed-loop predictive controller performance in terms of individual and collective generated power.

5. Conclusions

The main purpose of this work is to study the ability of IODMD and the ideas behind the Koopman Operator to build reduced order models for wind farm control strategies suitable for the design of predictive controllers.

The three main contributions achieved with this work are (1) to model, from a pure data driven perspective, wake redirection control by yaw misalignment (2) make use of the ideas motivated by the Koopman operator theory in the context of modelling for wind farm control strategies and (3) design and implement in a high fidelity simulator a MPC to track a collective power reference.

It is shown that a ROM built with streamwise velocity information u with 37 states is able to both predict the wake dynamics and provide an accurate mapping to the power produced at both turbines. The wake is predicted with an average NRMSE of 4%, demonstrating the ability of a linear state space ROM in predicting the behaviour of a non linear high dimensional system, within a certain operational domain. Moreover, the model reproduces power generated in the downstream turbine with a VAF of 88.40% and in the upstream turbine with a VAF of 99.12%.

Furthermore, using other flow field information, including non linear functions of the velocity field, leads to improved mapping from states to power output. Using u^2 leads to a ROM with 26 states and a VAF of the power captured at the second turbine of 89.63%, a small increase of 1.23%. Other non linear observables, such as the sum of the squares of velocity components, namely $u^2 + v^2$ and $u^2 + v^2 + w^2$, show minor benefits in the order of 1% in VAF for the generator power of the second turbine.

Additionally, it is shown that the MPC controllers are able to embed the slow dynamics of the wind farm system, meaning that the aerodynamic interaction between turbines is taken into account for the optimal control action computation. The open-loop implementation shows that the MPC acts anticipatedly, varying the control action 2 to 3 minutes before the new reference sets in.

The final closed-loop implementation shows that by implementing a simple estimator and restricting the yaw angle rate to avoid abrupt control action variations, a smooth solution for the collective power tracking can be achieved.

Future work will investigate the application of IODMD and similar data driven techniques to model other wind farm control strategies with the goal of not only designing controllers but also gaining insight into the dynamics of more complex strategies. In addition, using other type of models, such as Linear Parameter Varying (LPV), provide a possible route to better capture the non linear dynamics at various operating points. Moreover, different control problem can be formulated, namely controlling loads in each turbine or redirecting the center of the wake.

References

[1] J. Annoni. *Modeling for Wind Farm Control*. PhD thesis, University of Minnesota, May 2016.

[2] J. Annoni, P. M. O. Gebraad, and P. Seiler. Wind farm flow modeling using an input-output reduced-

order model. *2016 American Control Conference (ACC)*, pages 506–512, 2016.

[3] J. Annoni and P. Seiler. A low-order model for wind farm control. *2015 American Control Conference (ACC)*, pages 1721–1727, 2015.

[4] B. Brunton, L. Johnson, and N. K. Jeffrey Ojemann. Extracting spatial-temporal coherent patterns in large-scale neurural recordings using dynamic mode decomposition. *Journal of Neuroscience Methods*, 258:1–15, January 2016.

[5] F. Campagnolo, V. Petrović, C. Bottasso, and A. Croce. Wind tunnel testing of wake control strategies. pages 513–518, 07 2016.

[6] M. J. Churchfield, S. Lee, J. Michalakes, and P. J. Moriarty. A numerical study of the effects of atmospheric and wake turbulence on wind turbine dynamics. *Journal of Turbulence*, 13:N14, 2012.

[7] P. Fleming, P. Gebraad, S. Lee, J. W. Wingerden, K. Johnson, M. Churchfield, J. Michalakes, P. Spalart, and P. Moriarty. Evaluating techniques for redirecting turbine wake using sowfa. *Renewable Energy*, 70:211–218, 10 2014.

[8] P. Fleming, J. King, K. Dykes, E. Simley, J. Roadman, A. Scholbrock, P. Murphy, J. K. Lundquist, P. Moriarty, K. Fleming, J. van Dam, C. Bay, R. Mudafort, H. Lopez, J. Skopek, M. Scott, B. Ryan, C. Guernsey, and D. Brake. Initial results from a field campaign of wake steering applied at a commercial wind farm - part 1.

[9] G. H. Golub and C. F. Van Loan. *Matrix Computations*. The Johns Hopkins University Press, third edition, 1996.

[10] J. H. Tu, C. W. Rowley, D. M. Luchtenburg, S. L. Brunton, and J. Nathan Kutz. On dynamic mode decomposition: Theory and applications. *Journal of Computational Dynamics*, 1(2):391–421, 2014.

[11] G. V. Iungo, C. Santoni-Ortiz, M. Abkar, F. Porté-Agel, M. A. Rotea, and S. Leonardi. Data-driven reduced order model for prediction of wind turbine wakes. *Journal of Physics: Conference Series*, 625:012009, jun 2015.

[12] T. Katayama. *Subspace Methods for System Identification*. Springer, 2005.

[13] I. Kevrekidis, C. Rowley, and M. Williams. A kernel-based method for data-driven koopman spectral analysis. *Journal of Computational Dynamics*, 2:247–265, 05 2016.

[14] I. Komusanac, G. Brindley, and D. Fraile. Wind energy in euope: Trends and statistics. Technical report, Global Wind Energy Council, February 2020.

[15] B. O. Koopman. Hamiltonian systems and transformation in hilbert space. *Proceedings of the National Academy of Sciences*, 17(5):315–318, 1931.

[16] J. Kutz, J. Proctor, and S. Brunton. Applied koopman theory for partial differential equations and data-driven modeling of spatio-temporal systems. *Complexity*, 2018:1–16, 12 2018.

[17] H. Lu and D. M. Tartakovsky. Predictive accuracy of dynamic mode decomposition. *arXiv: Numerical Analysis*, 2019.

[18] W. Munters and J. Meyers. An optimal control framework for dynamic induction control of wind farms and their interaction with the atmospheric boundary layer. *Philosophical Transactions of the Royal Society of London, Series A: Mathematical, Physical and Engineering Sciences*, 375(2091), April 2017.

[19] W. Munters and J. Meyers. Towards practical dynamic induction control of wind farms: analysis of optimally controlled wind-farm boundary layers and sinusoidal induction control of first-row turbines. *Wind Energy Science*, 3(1):409–425, June 2018.

[20] J. Proctor and P. Eckhoff. Discovering dynamic patterns from infectious disease data using dynamic mode decomposition. *International Health*, January 2015.

[21] J. L. Proctor, S. L. Brunton, and J. N. Kutz. Dynamic mode decomposition with control. *SIAM Journal on Applied Dynamical Systems*, 15(1):142–161, Jan 2016.

[22] H. Ritchie. Renewable energy. *Our World in Data*, 2017.

[23] C. Rowley, I. Mezic, S. Bagheri, P. Schlatter, and D. Henningson. Spectral analysis of nonlinear flows. *Journal of Fluid Mechanics*, 641:115 – 127, 12 2009.

[24] P. Schmid. Dynamic mode decomposition of numerical and experimental data. *Journal of Fluid Mechanics*, 656:5–28, August 2010.

[25] P. Schmid, K. E. Meyer, and O. Pust. Dynamic mode decomposition and proper orthogonal decomposition of flow in a lid-driven cylindrical cavity. *8th International Symposium on Particle image Velocimetry - PIV09*, August 2009.

[26] M. Steinbuch, W. Boer, de, O. Bosgra, S. Peeters, and J. Ploeg. Optimal control of wind power plants. *Journal of Wind Engineering and Industrial Aerodynamics*, 27(1-3):237–246, 1988.

[27] T. J. van den Boom and T. C. Backx. *Model Predictive Control*. Delft University of Technology, Delft Center for Systems and Control, September 2005. Lecture Notes for the course SC4060.

[28] J. W. van Wingerden, P. A. Fleming, T. Göçmen, I. Eguinoa, B. M. Doekemeijer, K. Dykes, M. Lawson, E. Simley, J. King, D. Astrain, M. Iribas, C. L. Bottasso, J. Meyers, S. Raach, K. Kölle, and G. Giebel. Expert elicitation on wind farm control, 2020.

[29] M. Viberg. Subspace-based methods for the identificaiton of linear time-invariant systems. *Automatica*, 31(12):1835–1851, 1995.

[30] M. Williams, I. Kevrekidis, and C. Rowley. A data-driven approximation of the koopman operator: Extending dynamic mode decomposition. *Journal of Nonlinear Science*, 25, 08 2014.

[31] F. Zahle, R. Bitsche, T. Ki, A. Yde, L. C. Henriksen, M. H. Hansen, J. Blasques, M. Gaunaa, and A. Natarajan. *The DTU 10-MW Reference Wind Turbine*. Section for Aeroelastic Design and Section for Structures Technical University of Denmark DTU Wind Energy – Risø Campus, 2013.